Time-dependent lepto-hadronic modeling of the emission processes in blazar jets

S. Gasparyan[1], D. Bégué[2,3] and N. Sahakyan[1,4,5]

[1] *ICRANet-Armenia, Marshall Baghramian Avenue 24a, Yerevan 0019, Armenia*
[2] *Department of Physics, Bar Ilan University, Ramat-Gan 52900, Israel* *
[3] *Max-Planck-Institut für extraterrestrische Physik, Giessenbachstrasse, D-85748 Garching, Germany*
[4] *ICRANet, P.zza della Repubblica 10, 65122 Pescara, Italy*
[5] *ICRA, Dipartimento di Fisica, Sapienza Universita' di Roma, P.le Aldo Moro 5, 00185 Rome, Italy*
* *E-mail: sargisgyan@gmail.com*

The recent associations of neutrino events with blazars (e.g. TXS 0506+056, 3HSP J095507.9+355101) provided a unique opportunity to study the possible physical connection between the multiwavelength electromagnetic and neutrino emissions. We present *SOPRANO*, a new conservative implicit kinetic code which follows the time evolution of the isotropic distribution functions of protons, neutrons and the secondaries produced in photo-pion and photo-pair interactions, alongside with the evolution of photon and electron/positron distribution functions. In the current work, we apply *SOPRANO* to model the broadband spectrum of TXS 0506+056, 3HSP J095507.9+355101 and 3C 279 blazars. It was possible to constrain main physical parameters within both a pure hadronic and lepto-hadronic scenarios.

Keywords: Radiation mechanisms; non-thermal–quasars; individual; TXS 0506+056, 3HSP J095507.9+355101 and 3C 279 – galaxies; jets – gamma-rays; galaxies

1. Introduction

In recent years, the discovery of very high energy neutrinos of astrophysical origin by the IceCube experiment[1–3] has opened a new window on very high energy sources such as gamma-ray bursts (hereafter GRBs), active galactic nuclei (AGNs) and tidal disruption events (TDEs). In 2017, the very high energy neutrino IceCube 170922A[4] and its further association (confidence level of 3.5σ) with the blazar TXS 0506+056[5] made clear that high energy protons, neutron and even possibly nucleons have an important role to play in the dynamics and the radiation of relativistic jets.[6–8]

In the forthcoming years, it is expected that many more crucial data will become available for high energy sources at all wavelengths, but more importantly at very high energy. For instance, the MAGIC collaboration recently reported the first observations of a GRB at energies above TeV with its observation of 190114C,[9] and several more are expected to be observed with CTA.[10,11] In addition, upgrades of existing neutrino facilities, with e.g. IceCube-Gen2,[12] as well as new experiments such as P-one,[13] KM3Net[14] and the Baikal-GVD,[15] will allow for increasingly more

*Current address.

sensitive searches of the origin of very high energy neutrinos.[16] Those experiments should also help to establish more firm coincidental observations of neutrino bursts with identified electromagnetic counterparts, thus allowing for models to be tested, constrained, challenged and eventually ruled out.

In order to understand observations and constrain models of emission able to explain very high energy neutrinos, it is necessary to perform self-consistent simulations of the time evolution of hadrons distribution functions, together with following the evolution of the photon and lepton distribution functions. This is a challenging task since 1- the number of distributions is much larger (from two to fourteen although some are trivial), 2- all equations describing the time evolution of particle distribution functions are coupled in a non-trivial (and non-linear) way by many complex processes that 3- have different time scales, requiring an implicit time discretization. The high number of distribution functions comes from the fact that we also wish to follow the cooling and emission of charged secondaries (pion and muons), preventing us from using semi-analytical expressions for the production rate of neutrinos, see *e.g.*[17]

Over the years, several groups have developed numerical models to estimate leptons, hadron and photon distribution functions in order to make predictions to explain observations, either under the steady state approximation[18–21] or for the fully time dependent equations either for leptons only[22] or adding protons.[23–28] In this paper, we present our approach to the problem: a modular code solving the time dependent isotropic kinetic equations which preserves the total energy of the system as well as the number of particles where needed. The code structure is modular such that processes can be added easily (or removed). It is also implicit so numerical stability is achieved at all time.

The paper is organised as follows. In Section 2, we detail the processes included in our numerical code and the associated kinetic equation. In Section 3, we provide elements of the numerical discretizations in energy and time. In Section 4 we present examples of the theoretical modelings obtained by *SOPRANO*. In particular, we model the spectra of TSX 0506+056, 3HSP J095507.9+355101 and of 3C 279. The conclusion follows.

2. *SOPRANO*: Simulator of Processes in Relativistic AstroNomical Objects

In its current version, the code evolves in time the isotropic kinetic equations for photons, electrons and positrons (considered as one species, see below), protons, neutrons, charged and neutral pions, muons, neutrino and anti-neutrino of all flavors. We summarize here all terms appearing in the kinetic equation for all particle species. For the cross-sections used in SOPRANO see.[29] In the photon distribution function, we assign $n_{\rm ph}$ to be the number of photons per unit volume per hertz. We further define $N_{\rm i}$ to be the number of particles of species i per unit volume per unit Lorentz factor of particle i. Here i can be all leptons and all hadrons. Then, we

define N_{ν_i} the number of neutrinos of flavour i per units volume per GeV. Finally, for the sink and source terms we assign Q and S, respectively. The contribution of inverse Compton scattering is noted R_{IC} for the photons and is a cooling term for the leptons.

- *Photons :* they are created by synchrotron radiation from all charged particles, and by π_0 decay. They are absorbed by pair production and redistributed in energy by inverse Compton scattering. We neglect the absorption of photons in the photo-pion and photo-pair processes. The resulting kinetic equation takes the form

$$\frac{\partial n_{\rm ph}}{\partial t} = -S_{\gamma\gamma\to e^+e^-} + Q_{\pi_0} + R_{\rm IC} + \sum_i Q^i_{\rm synch} \tag{1}$$

- *Leptons :* electron and positrons are considered a single species. They are created by muon decay μ, by photo-pair production and photon pair production. The also undergo synchrotron cooling such that the final kinetic equation reads

$$\frac{\partial N_{\rm e^\pm}}{\partial t} = Q_\mu + Q_{p\gamma\to e^+e^-} + Q_{\gamma\gamma\to e^+e^-} C_{\rm IC} + C_{\rm synch} \tag{2}$$

- *Protons :* protons undergo cooling via synchrotron emission, Bethe-Heitler photo-pair production and via photo-pair production. They are produced by photo-pair interaction with neutron, and disappear for a fraction of photo-pair interaction. The kinetic equation takes the form

$$\frac{\partial N_p}{\partial t} = C_{p\gamma\to p\pi} + C_{p\gamma\to e^+e^-} + C_{\rm synch} - S_{\gamma p\to n\pi} + Q_{\gamma n\to p\pi} \tag{3}$$

- *Neutron :* Neutron are produced in photo-pion production and disappear in photo-pion interactions. The kinetic equation takes the form

$$\frac{\partial N_n}{\partial t} = -S_{n\gamma\to p\pi} + Q_{p\gamma\to n\pi} + C_{n\gamma\to n\pi} \tag{4}$$

- *Charged pions :* π_+ and π_- are produced by photo-pair production. Then, they cool via synchrotron emission and decay. The kinetic equation for both species takes the form

$$\frac{\partial N_{\pi_\pm}}{\partial t} = Q_{p\gamma\to\pi} + Q_{n\gamma\to\pi} - S_\pi + C_{\rm synch} \tag{5}$$

  We note that we solve the kinetic equation independently for both species, since the branching ratio in photo-pion production are different for negative and positive pions.
- *Neutral pions :* the π_0 kinetic equation is similar to that of charged pions but without synchrotron cooling.

- *Muons :* Muons are produced by the decay of charged pions. They are also cooled by the synchrotron process and they decay. Therefore, the kinetic equation is

$$\frac{\partial N_\mu}{\partial t} = Q_{\pi_\pm} - S_\mu + C_{\rm synch} \tag{6}$$

- *Neutrinos and anti-neutrinos:* neutrinos and anti-neutrinos are produced in the decay of pions and of muons. We consider all 2 flavours ζ

$$\frac{\partial N_{\nu,\zeta}}{\partial t} = Q_{\pi_\pm} + Q_\mu \tag{7}$$

3. Numerical Discretization

The SOPRANO follows the evolution of distribution functions as a function of time under the following simplificative assumptions: i) space is infinite and homogeneous, ii) distribution functions are isotropic. For disretization, SOPRANO uses a flavour of finite volume approximation based on the discontinuous Galerkin method. This method fits nicely for solving integro-differential equations.

3.1. *Energy discretization*

In order to numerically solve the kinetic equations presented in Section 2, a numerical grid for the energy of all particles is introduced. The grid element are equally space in logarithmic of the energy.[a] The grid characteristics for each types of particle are given by Table 1. We use the approach of the discontinuous Galerkin method. On each energy cell I, we approximate the distribution function by a polynomial. In the current version we restraint to first order and consider the Legendre polynomial as basis function. Therefore, on each energy cell I, the distribution function is approximated by

$$N_{\rm i}^I(x) = N_{\rm i,0}^I L_0^I(x) \tag{8}$$

where the first order Legendre polynomial on the energy cell I is

$$L_0^I = \frac{1}{\sqrt{x_{I+\frac{1}{2}} - x_{I-\frac{1}{2}}}} \equiv \frac{1}{\sqrt{||I||}} \tag{9}$$

Here $x_{I\pm(1/2)}$ are the boundaries of energy cell I and where we introduced the additional notation $||I|| = (x_{I+1/2} - x_{I-1/2})$. An important properly of the Legendre polynomial is that

$$\int_I L_0^I dx = 1. \tag{10}$$

[a]Note that our numerical method do not require to have a uniform grid. Because it is based on finite volume, we can refine the grid in one or several energy bands of interest. In this way, we can provide more detailed results in those specific bands, while the rest of the domain is coarse for faster numerical estimation.

Table 1. Characteristics of the numerical grids used by SOPRANO for the numerical models of this work. The cells are equally space in logarithmic scale.

Particle	Number of cells	Minimum energy	Maximum energy
Photons	150	$\nu = 10^{-2}$Hz	$\nu = 10^{30}$ Hz
Leptons	130	$\gamma_{e\pm} = 1.2$	$\gamma_{e\pm} = 5 \times 10^{13}$
Hadrons	100	$\gamma_h = 1.2$	$\gamma_h = 10^{11}$
Neutrinos	100	$E_\nu = 10^{-3}$ GeV	$E_\nu = 10^{11}$ Gev

In the following we will use interchangeably $N_i^I \equiv N_{i,0}^I$. We seek the weak formulation of all kinetic equations presented below on all energy interval I. For this, we multiply both sides of the equation by L_0 and integrate over I. After simplification, we obtain a system of differential equations for all $N_{i,0}^I$. This specific discretization and the structure of the kinetic equation allows us to retrieve a numerical method which conserves energy and the number of particles when they are conserved.

3.2. *Temporal discretization*

Before discussing the temporal discretization, we note that the equation are non-linear in the distribution function for Compton scattering, pair production, photo-pion and photo-pair processes. We have decided to linearize the kinetic equation of photo-pion and photo-pair processes by assuming that the target photon-field is equal to the one at the previous time step, effectively making those process linear in the distribution function. For all leptonic processes,[b] we preserve the non-linearity of the kinetic equations and solve at each time step a non-linear system via Newton-Raphson iteration. The temporal evolution of the distribution function is performed with the implicit Euler.

The computation of one time step is done in the following form

(1) solve the linear kinetic equation for the protons since for photo-pion and photo-pair processes the photon distribution function is assumed to be known and given by its value at time t. The pairs created in the photo-pair processes are saved to be use as a source term in the leptonic computation.
(2) compute the decay and cooling (when required) of pions and muons. The pairs and photons created in the muon and pion decay are used as source terms in the leptonic computation.
(3) perform the fully implicit leptonic computation with the source term computed in the two previous steps.

4. Modeling of Blazar SEDs

The code *SOPRANO*, described in Section 2, is used to model the multiwavelength SEDs of TXS 0506+056, 3HSP J095507.9+355101 and 3C 279. Two of these sources,

[b]This is true for all process but synchrotron which is linear in the distribution function.

TXS 0506+056 and 3HSP J095507.9+355101, coincide in space and time with the IceCube 170922A[4] and IceCube 200107A[30] events, respectively. The other source, 3C 279, shows a prominent flare in the γ-ray band. In all modelings, the emission region assumed to be a sphere with a radius of R' which is moving with a bulk Lorentz factor of $\Gamma \sim \delta$, carries a magnetic field with an intensity of B' and a population of relativistic particles. The magnetic jet luminosity is defined as

$$L_{\rm B} = \pi c R'^2 \delta^2 \frac{B'^2}{8\pi}, \tag{11}$$

while for protons and electrons as follows:

$$L_{\rm p} = \pi R'^2 \delta^2 m_{\rm p} c^3 \int \gamma_{\rm p} Q'_{\rm p}(\gamma_{\rm p}) \gamma_{\rm p}, \tag{12}$$

$$L_{\rm e} = \pi R'^2 \delta^2 m_{\rm e} c^3 \int \gamma_{\rm e}\, Q'_{\rm e}(\gamma_{\rm e})\, d\gamma_{\rm e}, \tag{13}$$

where c is the speed of light, $m_{\rm p}$ and $m_{\rm e}$ are the proton and electron masses, while $Q'_{\rm p}$ and $Q'_{\rm e}$ refer to proton and electron injection spectra, with the following forms:

$$Q'_{\rm p}(\gamma_{\rm p}) = Q'_{0,p} \gamma_{\rm p}^{-\alpha_{\rm p}} \qquad \gamma_{\rm p} < \gamma_{\rm p,max}. \tag{14}$$

$$Q'_{\rm e}(\gamma_{\rm e}) = \begin{cases} Q'_0 \gamma_{\rm e}^{-\alpha_{\rm e}} \exp\left(-\dfrac{\gamma_{\rm e}}{\gamma_{\rm e,cut}}\right) & \gamma_{\rm e,min} \le \gamma_{\rm e} \le \gamma_{\rm e,max}, \\ 0 & \text{otherwise}, \end{cases} \tag{15}$$

where $\gamma_{\rm e,min}$ is the minimum injection Lorentz factor. All primed quantities refer to the comoving frame. The distribution functions of protons and electrons evolve via cooling and via interaction with photons, producing different signatures in the broadband spectrum. Our aim is to identify those signatures and use them to constrain the emission mechanism within the framework of different scenarios. We also assume that the injection power-law indexes are such that $\alpha_{\rm e} = \alpha_{\rm p}$. Once injected in the emitting region, particles interact with the magnetic field and with the photons, producing secondary particles, which themselves interact, radiate and decay, shaping the broadband SED. The low energy component is interpreted as the synchrotron emission of the primary electrons while the HE component is modelled either within a pure hadronic model(hereafter HM) or a hybrid lepto-hadronic (hereafter hybrid) model e.g.[31,32] For the HM, the high energy peak on SED is formed due to the proton synchrotron emission, however in the hybrid model, the high energy peak is explained by leptonic processes and proton synchrotron emission is required to be subdominant. The proton content is obtained by maximizing the neutrino flux at PeV energies, which is constrained by the radiation from the secondaries produced by the Bethe-Heithler and photo-pion processes. Indeed, it has long been speculated that efficient neutrino production is associated with efficient Bethe-Heithler process, creating a population of HE pairs, which can over-shine the tight constraints in the X-ray band e.g., order of minutes.[33] The system of kinetic equations is evolved for

one dynamical time scale $t'_{\rm dyn} \sim R'/c$ considering the magnetic field to be constant, and taking into account all relevant processes for particles interactions. Having estimated the model parameters of each blazar SEDs, the corresponding neutrino flux can be derived. The flux of muon neutrino, $F_{\nu_\mu}(E_{\nu_\mu})$, in all considered scenarios is shown by the light blue line in Figures 1-3. When available, the neutrino flux is compared with the limit imposed by the IceCube detector. This flux can be transformed to the expected observed number of neutrinos in the IceCube detector using its averaged effective area $A_{\rm eff}(\mathrm{E}_\mu)$, which is mostly a function of the incident neutrino energy. For 3HSP J095507.9+355101 and 3C 279, the average area from[34] was considered, while for TXS 0506+056 we used the area released after the observation of IceCube-170922A.[c] The effective area increases with energy and reaches its maximal value for energies above several hundreds of PeV. The expected number of muon neutrinos and anti-neutrinos is computed through

$$N_{\nu_\mu+\bar{\nu}_\mu} = t_{\rm exp} \int_{E_{\rm min,\nu_\mu}}^{E_{\rm max,\nu_\mu}} F_{\nu_\mu}(E_{\nu_\mu})\, A_{\rm eff}(\mathrm{E}_{\nu_\mu})\, dE_{\nu_\mu} \tag{16}$$

where the minimum and maximum energy of the neutrinos are $E_{\rm min,\nu_\mu} = 100$ GeV and $E_{\rm max,\nu_\mu} = 10^9$ GeV, respectively, chosen to correspond the limits for the effective area. The expected number of neutrino events depends on the duration of the source activity, $t_{\rm exp}$, over which the neutrinos are emitted. The neutrino oscillation, within the quasi-two neutrino oscillation assumption, is taken into account by

$$N^{obs}_{\nu_\mu} = 0.575 N_{\nu_\mu} + 0.425 N_{\nu_e}, \tag{17}$$

where $N^{obs}_{\nu_\mu}$ is the observable distribution of muon neutrinos, while, N_{ν_μ} and N_{ν_e} are the emitted muon and electron neutrino distributions.[35]

5. Results

The results of the SEDs modeling are shown in Fig. 1-3 with the Table 2 and 3.

TXS 0506+056: Two different periods are chosen for modelling: the single neutrino detection period,[4] and the historical neutrino flaring period.[5] The modeling results are shown in Figure 1 and Table 2. Panels a) and b) of Figure 1 represent the modeling of SED of the single neutrino event period, while panel c) and d) show flare for historical neutrino flare SED modelings. The multiwavelength data from[4] are modeled within a HM scenario in panel a). The corresponding model parameters are given in Table 2. The sum of all components, represented by the blue line in the top left panel of Figure 1, satisfactorily explains the observed data. The model overpredicts the radio data, but by taking into account the synchrotron self-absorption effect,[29] the model is in agreement with the data. The modeling parameters given in the first column of Table 1 are in the range of similar estimations for blazars in general and for TXS 0506+056 in particular. A Doppler factor $\delta = 20$ and a radius

[c] https://icecube.wisc.edu/science/data-releases/

$R' = 2.5 \times 10^{15}$ cm were used in our modeling. This is in agreement with the limits on the variability time of 10^5s presented in.[36] We note that when $\delta = 10$ or 15, the data can also be well reproduced by the model. The initial injection power-law index of the emitting electrons is $\alpha_e = 2.1$, a value that can be formed by shock accelerations, *e.g.*[37] Due to the high magnetic field, $B = 80$ G, electrons are in the fast cooling regime and their distribution function is a power-law with index $\alpha_e + 1$. The initial electron distribution extends up to $\gamma_{\rm cut} = 2.4 \times 10^3$ (~ 1 GeV) which is representative of the acceleration and cooling time scales. Instead, protons cool less efficiently and they could be accelerated up to much higher energies, *i.e.* $\gamma_{\rm max} = 10^9$ (9.4×10^{17} eV), see.[29]

As an alternative model to HM or leptonic models, the hybrid model is also applied to the SED of TXS 0506+056, shown in panel b) of Figure 1. The model parameters are given in the second column of Table 2. The blue dashed lines represent the time evolution of the spectrum in selected numerical steps, which builds and forms the overall SED, represented by the solid blue line after one dynamical time scale. The synchrotron component peaking between 1-10 eV is up-scattered by the relativistic electrons to produce the HE and VHE component. In contrast to HM scenario, the magnetic field in the emitting region is $B = 0.57$G significantly lower, therefore, electrons with Lorentz factor $\gamma_{\rm e,min} = 10^3$ are not substantially cooled within one dynamical time scale. For this hybrid model, protons do not directly contribute to the observed SED, instead the contribution of secondary electron-positrons dominates in the X-ray band, which puts constraints on the proton luminosity and as a consequence the neutrino luminosity. For example, if one increases by 1.5 times the proton luminosity, the model would overshoot the X-ray data, as shown by the dotted-dashed blue line in panel b) of Figure 1.

Further the results of the SED modeling obtained during the historical neutrino flare of TXS 0506+056 is presented. Unfortunately, when 13 ± 5 neutrinos were observed between October 2014 and March 2015,[5] the multiwavelength coverage is scarce. Yet, the flux upper limit of $F < 9.12 \times 10^{-12}$erg cm^{-2} s^{-1} derived from Swift BAT observations[38] introduces substantial difficulties for a one-zone modeling. Indeed, the predicted number of neutrino events cannot be matched to the IceCube observations[38] and[39] have shown that only few neutrino events could be detected under different optimistic considerations for the emitting region and for the target photon field (internal or external to the jet). Matching together the observed multiwavelength data and the neutrino data seems to require two zone models with more free parameters.[38,39]

To accommodate the X-ray limit and try to account for the neutrino flux during this flare, two different assumptions on the proton distribution function are made. On the one hand, radiation from the secondaries can be constrained to be dominant in the MeV band, in which there are no observational constraint. On the other hand, radiation from the secondaries could be dominant in the GeV band and produce the second HE hump. The SEDs of these two models are respectively shown in panels c) and d) of Figure 1, with data from.[39] Those two models lead to two very

different sets of parameters for the emitting region, see column 3 and 4 of Table 2. The first model requires a large radius $R' = 10^{17}$cm and a slowly moving jet with Doppler factor $\delta = 10$, while the second model necessitates those parameters to be $R' = 10^{15}$cm and $\delta = 15$. The required magnetic field also significantly differs between these two models with $B = 35$G for the first model, to be compared to $B = 0.65$G for the second one. The first model tends to reproduce the neutrino flux, albeit produces the peak at lower energies. The second model puts the neutrino peak at larger energy, but is not able to reproduce the observed neutrino number. In both interpretations, it is clear that the upper limit in the X-ray band imposes strong constraints on the photon spectrum, which in turn limits the proton content in the jet. Considering larger proton luminosity would lead to over-estimate both the observed γ-ray flux and the X-ray upper limit.

Table 2. Parameter sets used for modeling the SEDs of TXS 0506+056, observed in 2017 and during the neutrino flare in 2014-2015. The electon, proton and magnetic luminosities are also given.

	TXS 0506+056: 2017		TXS 0506+056: 2014-2015	
	Hadronic	Lepto-hadronic	Hadronic	Lepto-hadronic
δ	20	20	15	10
$R/10^{15}$ cm	2.5	10	1	100
$B[G]$	80	0.57	35	0.65
$\gamma_{\rm e,min}$	100	1000	2×10^2	9×10^3
$\gamma_{\rm e,cut}$	2.4×10^3	4.5×10^4	10^4	$=\gamma_{\rm e,max}$
$\gamma_{\rm e,max}$	3×10^4	6×10^4	8×10^4	8×10^4
$\alpha_{\rm e}$	2.1	2.0	2.0	2.0
$\alpha_{\rm p} = \alpha_{\rm e}$	2.1	2.0	2.0	2.0
$\gamma_{\rm p,min}$	1	1	1	1
$\gamma_{\rm p,max}$	10^9	10^6	2×10^8	1.2×10^5
$L_{\rm e}$ (erg s^{-1})	2.2×10^{44}	9.3×10^{44}	2.8×10^{44}	5.3×10^{44}
$L_{\rm B}$ (erg s^{-1})	6.0×10^{46}	4.9×10^{43}	10^{45}	1.6×10^{45}
$L_{\rm p}$ (erg s^{-1})	2.1×10^{47}	2.6×10^{50}	3.4×10^{47}	4.9×10^{52}

From the jet energetic perspective, the total jet luminosity in the case of TXS 0506+056, for the proton synchrotron model, shown on panel a) of Figure 1, is $L_{\rm tot} = L_{\rm p} + L_{\rm e} + L_{\rm B} = 2.7 \times 10^{47}\,{\rm erg\,s^{-1}}$, which exceeds by one order of magnitude the Eddington luminosity of $\simeq 4 \times 10^{46}{\rm erg\,s^{-1}}$ for a black hole mass of $3 \times 10^8\,M_\odot$, as estimated for TXS 0506+056 using the absolute R-band magnitude.[40] This is in agreement with previous studies suggesting that in the case of proton synchrotron models or models producing a high neutrino flux, the required jet luminosity exceeds that of the Eddington limit.[41] Within the hybrid model, matching the neutrino flux with the neutrino event of TXS 0506+056, displayed on panel b) of Figure 1, requires the jet luminosity to be $\sim 10^{50}\,{\rm erg\,s^{-1}}$, significantly exceeding that of the Eddington luminosity. Although the Eddington luminosity is not a strict limit and super-Eddington luminosities were previously reported,[42] this value is extremely large. On the other hand, for the neutrino flare in 2014-2015, when assuming that

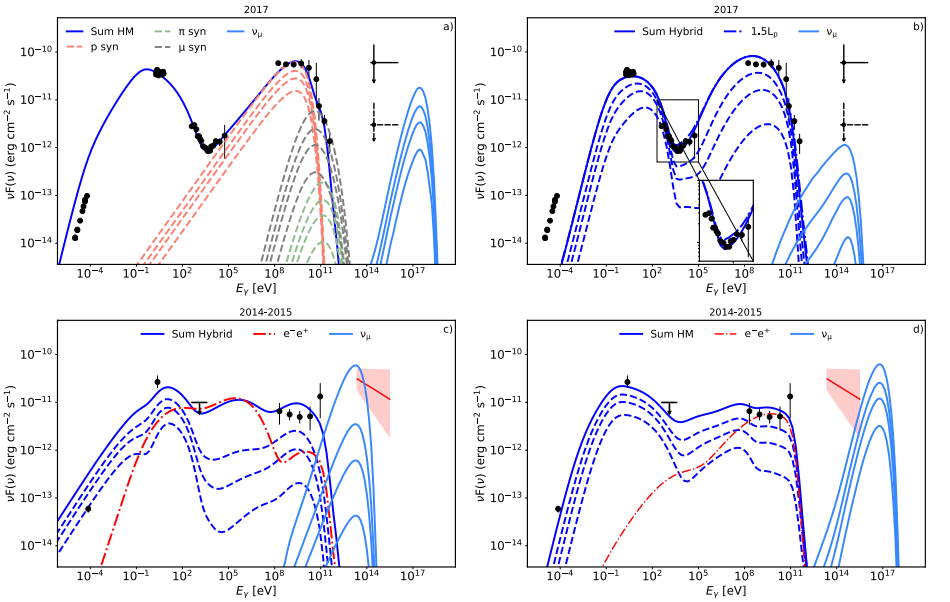

Fig. 1. The multiwavelength SED of TXS 0506+056 during the neutrino emission in 2017 (upper panels) and during the neutrino flare in 2014-2015 (lower panels) modeled within the hadronic and lepto-hadronic hybrid scenarios. The solid blue line in all plots represents the sum of all components which has been corrected for EBL absorption considering the model of.[43]

the emission from the secondary pairs solely dominates in the X-ray and γ-ray bands, an unrealistically high luminosity of $\sim 10^{52}$erg s^{-1} is obtained. Indeed, matching the high neutrino flux with the large radius (10^{17} cm) imposed by the modeling in this case, requires a large protons density, hence the too large proton luminosity. In the alternative interpretation, when the emission from the secondary pairs dominates in the GeV band, a modest luminosity of 3.4×10^{47} erg s^{-1} is estimated.

The expected numbers of neutrinos during the 6 months flare of TXS 0506+056 are 0.43 and 0.23 for the hadronic and hybrid scenarios, respectively. During the 2014-2015 neutrino flare, our most optimistic models predict 3.0-3.3 neutrinos for a 6 months exposure time (note however that the IceCube observational window was $\sim$ 110 days). Our results are in agreement with previous estimations for TXS 0506+056 and confirm that within a one-zone scenarios, 13 ± 5 events from the direction of TXS 0506+056 cannot be explained.[38,39]

3HSP J095507.9+355101: It is the first time that the jet of an extreme blazar is associated with a neutrino event,[30] straightening the assumption that the jets of this blazar type are potential sites for cosmic rays and even ultra-high energy cosmic ray acceleration.[44]

The SED of 3HSP J095507.9+355101 is shown in Figure 2, where the multiwavelength data are from.[45] Optical, UV and X-ray data were acquired on the 8$^{\text{th}}$, 10$^{\text{th}}$ and 11$^{\text{th}}$ of January. However, since the data taken on the 8$^{\text{th}}$ and 11$^{\text{th}}$ of January

seem to have the same flux and spectral shape,[46] we only model the data from the 8$^{\rm th}$. The lack of available multiwavelength data does not allow to constrain the low and high energy peaks, which hardens the estimation of the model free parameters. A hint of a $20-30$ minutes variability has been found in the NICER and NuSTAR data, but only at the $\sim 3.5\,\sigma$ level.[47] Therefore, the compactness of the emitting region cannot be constrained. In order to keep the generality, the SED of 3HSP J095507.9+355101 is modeled for two different parameter configurations. For the HM, we consider $R' = 3\times10^{14}$ cm and $\delta = 15$, while for the hybrid model we assume $R' \simeq 10^{16}$ cm and $\delta = 30$. The all estimated parameters are shown in Table 3.

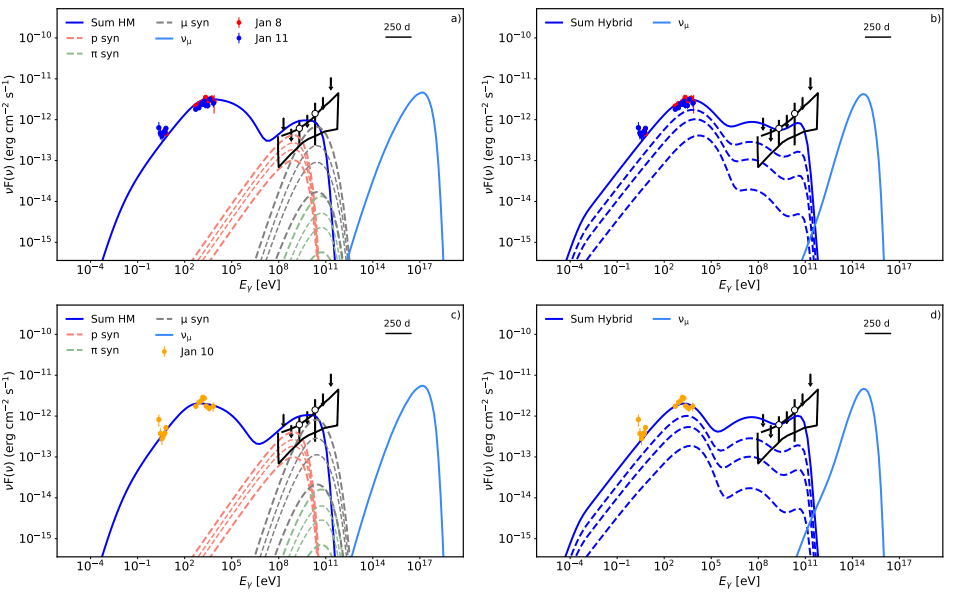

Fig. 2. The multiwavelength SEDs of 3HSP J095507.9+355101 on the the 8$^{\rm th}$ and the 11$^{\rm th}$ of January (panels a) and b) on the top raw) and on the 10$^{\rm th}$ of January (panels c) and d) on the bottom raw). The data are taken from.[45,46] The observed spectrum including all processes is shown by the solid blue line. All models (solid blue lines) have been corrected for EBL absorption considering the model of.[43]

The estimated muon neutrino rate for 3HSP J095507.9+355101, is within $6\times10^{-4} - 4.8\times10^{-3}$ per day. This implies that under this rate of emission, the expected number of neutrinos to be detected by IceCube in a time corresponding to the duration of the flare is very low. Such low neutrino estimation was obtained also by the authors of,[46] where they concluded that in the most promising scenarios, there is a $\sim 1\%$ to $\sim 3\%$ to observe one neutrino over the time characteristic of the long-term emission of 3HSP J095507.9+355101 (years).

3C 279: The broadband emission from the powerful FSRQs 3C 279 at redshift $z = 0.536$ has characterized by high amplitude variability almost in all energy

bands e.g., order of minutes,[48] and in particular in the HE γ-ray band, which present the fastest variability. On the 16$^{\rm th}$ of June 2015, Fermi LAT observations showed that 3C 279 was in an exceptionally bright state. The flux increased up to 3.6×10^{-5} photon cm^{-2} s^{-1} with a flux doubling time on the order of 5 minutes.[49] IceCube performed a time-dependent neutrino signal search correlated with this γ-ray flare but no evidence for a signal was found.[50] We apply *SOPRANO* to model the SED of 3C 279 during its flare in the framework of the HM, when the second peak dominates by proton synchrotron emission. The parameters of our modeling are given in Table 3. Figure 3 shows the multiwavelength SED of 3C 279 taken from,[51] alongside with the results of our modeling. During the brightening, the X-ray emission of the source appears with a hard photon index < 1.50, smoothly connecting with the INTEGRAL data, described by a power-law with index 1.08.[51] In the HE γ-ray band, the spectrum presents a power-law with photon index 2.21 with a turn over.[52] We make the hypothesis that the HE component is produced from a single mechanism. In our modeling it is interpreted as proton synchrotron emission, represented by the red dashed lines in Figure 3. This interpretation requires that protons are accelerated up to $\gamma_{\rm p,max} = 2.1 \times 10^8$, see Table 3.

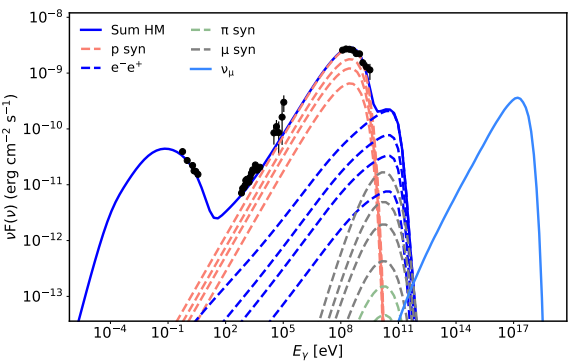

Fig. 3. The multiwavelength SED of 3C 279 during the exceptional flaring activity in 2015. The contribution of different particle emission is shown by dashed lines whereas the thick solid line represents the observed spectrum, corrected for EBL absorption considering the model of.[43]

The compactness of the emitting region implies a high efficiency for photo-pion and photo-pair interactions, which inject energetic secondary pairs. The contribution of these pairs dominates above ~ 10 GeV and peak at ~ 100 GeV, as can be seen by the blue dashed line in Figure 3. The synchrotron radiation of the primary electrons peaks at ~ 0.1 eV and its HE tail accounts for the observed optical/UV data. These data constrain the cut-off energy to be relatively low, $\gamma_{\rm e,cut} = 2.4 \times 10^2$, otherwise, for $B = 70$ G and $\delta = 55$, the synchrotron radiation would overshoot the observed flux in optical and UV bands. A similar hadronic modeling for this flare is presented in[51] and in.[53] The neutrino rate for the considered flaring period

is as high as 0.15 per day is estimated. However, for a relatively short period of the source activity, from minutes to one day, no neutrino events in the IceCube detector are expected, in agreement with.[50]

Table 3. Parameters used to model the multiwavelength SEDs of 3HSP J095507.9+355101 and 3C 279. The electron, proton and magnetic luminosity is also displayed.

	3HSP J095507.9+355101				3C 279
	January 8th		January 10th		
	Hadronic	Lepto-hadronic	Hadronic	Lepto-hadronic	Hadronic
δ	15	30	15	30	55
$R/10^{15}$ cm	0.3	10	0.3	10	0.32
$B[G]$	45	0.11	45	0.08	70
$\gamma_{\rm e,min}$	10^4	100	5×10^3	100	1
$\gamma_{\rm e,cut}$	6×10^5	2×10^6	2×10^5	7×10^5	2.4×10^2
$\gamma_{\rm e,max}$	9×10^5	6×10^6	5×10^5	6×10^6	4×10^2
$\alpha_{\rm e}$	1.9	2.0	1.9	2	1.8
$\alpha_{\rm p}=\alpha_{\rm e}$	1.9	2.0	1.9	2	1.8
$\gamma_{\rm p,min}$	1	1	1	1	1
$\gamma_{\rm p,max}$	9×10^8	10^6	9×10^8	10^6	2.1×10^8
$L_{\rm e}$ (erg s^{-1})	1.2×10^{44}	1.6×10^{44}	7.3×10^{43}	2.1×10^{44}	1.9×10^{44}
$L_{\rm B}$ (erg s^{-1})	1.5×10^{44}	4.1×10^{42}	1.5×10^{44}	2.2×10^{42}	5.7×10^{45}
$L_{\rm p}$ (erg s^{-1})	3.2×10^{46}	8.0×10^{50}	3.2×10^{46}	1.8×10^{51}	1.3×10^{49}

6. Conclusion

We have presented a new kinetic model of photo-hadronic and leptonic interactions aiming at studying the emission of optically thin (for Compton scattering) scenarios of relativistic sources (e.g., AGNs and GRBs). Our numerical solution of the kinetic equations for protons, neutrons, pions, muons, neutrinos, pairs, and photons conserves the total energy of the system as well as the number of particles where required. The code takes as an input the spectral injection rate of the particles (e.g., electrons and/or protons), and compute the time evolution of all relevant particles, including the secondaries, as they interact and cool, allowing the computation of the broadband emission spectrum at any given period. In this paper, we have applied *SOPRANO* to model the SEDs of three blazars, two of which are potentially associated to neutrino emission observed by IceCube. We have assumed different models for the production of the HE component and compute in all cases the expected number of muon neutrinos. The time-dependent nature of the code allowed to follow the evolution of all particles in one dynamical time scale and then assess the proton content in the jet by using the radiative spectrum of either secondaries or initial particles. This is necessary for the estimation of the expected number of neutrinos. Such time-dependent treatment of the particle evolution enabled us to constrain different scenarios of neutrino production by using the limits imposed by the observations in different bands.

References

1. IceCube Collaboration, Evidence for High-Energy Extraterrestrial Neutrinos at the IceCube Detector, *Science* **342**, p. 1242856 (November 2013).
2. M. G. Aartsen, et al., First Observation of PeV-Energy Neutrinos with IceCube, *Physical Review Letters* **111**, p. 021103 (July 2013).
3. M. G. Aartsen, et al., Characteristics of the Diffuse Astrophysical Electron and Tau Neutrino Flux with Six Years of IceCube High Energy Cascade Data, *Phys. Rev. Lett.* **125**, p. 121104 (Sep 2020).
4. IceCube Collaboration, et al., Multimessenger observations of a flaring blazar coincident with high-energy neutrino IceCube-170922A, *Science* **361**, p. eaat1378 (July 2018).
5. IceCube Collaboration, et al., Neutrino emission from the direction of the blazar TXS 0506+056 prior to the IceCube-170922A alert, *Science* **361**, 147 (July 2018).
6. M. C. Begelman, et al., Consequences of relativistic proton injection in active galactic nuclei, *The Astrophysical Journal* **362**, 38 (October 1990).
7. M. Sikora, et al., Radiation drag in relativistic active galactic nucleus jets, *Monthly Notices of the RAS* **280**, 781 (June 1996).
8. A. M. Atoyan and C. D. Dermer, Neutral Beams from Blazar Jets, *The Astrophysical Journal* **586**, 79 (Mar 2003).
9. MAGIC Collaboration, et al., Teraelectronvolt emission from the γ-ray burst GRB 190114C, *Nature* **575**, 455 (November 2019).
10. J. Kakuwa, et al., Prospects for detecting gamma-ray bursts at very high energies with the Cherenkov Telescope Array, *Monthly Notices of the RAS* **425**, 514 (September 2012).
11. Gilmore Rudy C., et al., IACT observations of gamma-ray bursts: prospects for the Cherenkov Telescope Array, *Experimental Astronomy* **35**, 413 (2013).
12. The IceCube-Gen2 Collaboration, et al., IceCube-Gen2: The Window to the Extreme Universe, *arXiv e-prints*, p. arXiv:2008.04323 (August 2020).
13. M. Agostini, et al., The Pacific Ocean Neutrino Experiment, *Nature Astronomy* **4**, 913 (September 2020).
14. S. Adrián-Martínez, et al., Letter of intent for KM3NeT 2.0, *Journal of Physics G Nuclear Physics* **43**, p. 084001 (August 2016).
15. C. Baikal-GVD, et al., Neutrino telescope in Lake Baikal: Present and Future, in *36th International Cosmic Ray Conference (ICRC2019)*, International Cosmic Ray Conference Vol. 36July 2019.
16. M. G. Aartsen, et al., Time-Integrated Neutrino Source Searches with 10 Years of IceCube Data, *Physical Review Letters* **124**, p. 051103 (February 2020).
17. S. Kelner and F. Aharonian, Energy spectra of gamma rays, electrons, and neutrinos produced at interactions of relativistic protons with low energy radiation, *Physical Review D* **78**, p. 034013 (2008).
18. K. Asano and S. Inoue, Prompt GeV-TeV Emission of Gamma-Ray Bursts Due to High-Energy Protons, Muons, and Electron-Positron Pairs, *The Astrophysical Journal* **671**, 645 (December 2007).
19. M. Böttcher, et al., Leptonic and Hadronic Modeling of Fermi-detected Blazars, *The Astrophysical Journal* **768**, p. 54 (May 2013).
20. M. Cerruti, et al., A hadronic origin for ultra-high-frequency-peaked BL Lac objects, *Monthly Notices of the RAS* **448**, 910 (March 2015).
21. A. Zech, et al., Expected signatures from hadronic emission processes in the TeV spectra of BL Lacertae objects, *Astronomy and Astrophysics* **602**, p. A25 (June 2017).

22. Y. G. Zheng, et al., A time-dependent particle acceleration and emission model: understanding particle spectral evolution and blazar flares, *Monthly Notices of the RAS* **499**, 1188 (October 2020).
23. A. Mastichiadis and J. G. Kirk, Self-consistent particle acceleration in active galactic nuclei., *Astronomy and Astrophysics* **295**, p. 613 (March 1995).
24. A. Pe'er and E. Waxman, Time-dependent Numerical Model for the Emission of Radiation from Relativistic Plasma, *The Astrophysical Journal* **628**, 857 (August 2005).
25. S. Dimitrakoudis, et al., The time-dependent one-zone hadronic model. First principles, *Astronomy and Astrophysics* **546**, p. A120 (October 2012).
26. C. Diltz, et al., Time Dependent Hadronic Modeling of Flat Spectrum Radio Quasars, *The Astrophysical Journal* **802**, p. 133 (April 2015).
27. S. Gao, et al., On the Direct Correlation between Gamma-Rays and PeV Neutrinos from Blazars, *The Astrophysical Journal* **843**, p. 109 (July 2017).
28. D. Kantzas, et al., A new lepto-hadronic model applied to the first simultaneous multiwavelength data set for Cygnus X-1, *Monthly Notices of the RAS* (October 2020).
29. S. Gasparyan, et al., Time-dependent lepto-hadronic modeling of the emission from blazar jets with SOPRANO: the case of TXS 0506+056, 3HSP J095507.9+355101 and 3C 279, *arXiv e-prints*, p. arXiv:2110.01549 (October 2021).
30. IceCube Collaboration, IceCube-200107A: IceCube observation of a high-energy neutrino candidate event, *GRB Coordinates Network* **26655**, p. 1 (January 2020).
31. M. Cerruti, et al., Leptohadronic single-zone models for the electromagnetic and neutrino emission of TXS 0506+056, *Monthly Notices of the RAS* **483**, L12 (February 2019).
32. S. Gao, et al., Modelling the coincident observation of a high-energy neutrino and a bright blazar flare, *Nature Astronomy* **3**, 88 (January 2019).
33. M. Petropoulou and A. Mastichiadis, Bethe-Heitler emission in BL Lacs: Filling the gap between X-rays and γ-rays, *Monthly Notices of the RAS* **447**, 36 (February 2015).
34. M. G. Aartsen, et al., Search for steady point-like sources in the astrophysical muon neutrino flux with 8 years of IceCube data, *European Physical Journal C* **79**, p. 234 (March 2019).
35. G. Fantini, et al., The formalism of neutrino oscillations: an introduction, *arXiv e-prints*, p. arXiv:1802.05781 (February 2018).
36. A. Keivani, et al., A Multimessenger Picture of the Flaring Blazar TXS 0506+056: Implications for High-energy Neutrino Emission and Cosmic-Ray Acceleration, *The Astrophysical Journal* **864**, p. 84 (September 2018).
37. R. Blandford and D. Eichler, Particle acceleration at astrophysical shocks: A theory of cosmic ray origin, *Physics Reports* **154**, 1 (October 1987).
38. A. Reimer, et al., Cascading Constraints from Neutrino-emitting Blazars: The Case of TXS 0506+056, *The Astrophysical Journal* **881**, p. 46 (August 2019).
39. X. Rodrigues, et al., Leptohadronic Blazar Models Applied to the 2014-2015 Flare of TXS 0506+056, *Astrophysical Journal, Letters* **874**, p. L29 (April 2019).
40. P. Padovani, et al., TXS 0506+056, the first cosmic neutrino source, is not a BL Lac, *Monthly Notices of the RAS* **484**, L104 (March 2019).
41. R. Xue, et al., On the Minimum Jet Power of TeV BL Lac Objects in the p-γ Model, *The Astrophysical Journal* **871**, p. 81 (January 2019).
42. Y.-F. Jiang, et al., Super-Eddington Accretion Disks around Supermassive Black Holes, *The Astrophysical Journal* **880**, p. 67 (August 2019).
43. A. Domínguez, et al., Extragalactic background light inferred from AEGIS galaxy-SED-type fractions, *Monthly Notices of the RAS* **410**, 2556 (February 2011).

44. P. Padovani, et al., Extreme blazars as counterparts of IceCube astrophysical neutrinos, *Monthly Notices of the RAS* **457**, 3582 (April 2016).
45. P. Giommi, et al., 3HSP J095507.9+355101: A flaring extreme blazar coincident in space and time with IceCube-200107A, *Astronomy and Astrophysics* **640**, p. L4 (August 2020).
46. M. Petropoulou, et al., Comprehensive Multimessenger Modeling of the Extreme Blazar 3HSP J095507.9+355101 and Predictions for IceCube, *The Astrophysical Journal* **899**, p. 113 (August 2020).
47. V. S. Paliya, et al., Multifrequency Observations of the Candidate Neutrino-emitting Blazar BZB J0955+3551, *The Astrophysical Journal* **902**, p. 29 (October 2020).
48. J. Aleksić, et al., MAGIC observations and multifrequency properties of the flat spectrum radio quasar 3C 279 in 2011, *Astronomy and Astrophysics* **567**, p. A41 (July 2014).
49. M. Ackermann, et al., Minute-timescale >100 MeV γ-Ray Variability during the Giant Outburst of Quasar 3C 279 Observed by Fermi-LAT in 2015 June, *Astrophysical Journal, Letters* **824**, p. L20 (June 2016).
50. R. Abbasi, et al., A Search for Time-dependent Astrophysical Neutrino Emission with IceCube Data from 2012 to 2017, *The Astrophysical Journal* **911**, p. 67 (April 2021).
51. E. Bottacini, et al., 3C 279 in Outburst in 2015 June: A Broadband SED Study Based on the INTEGRAL Detection, *The Astrophysical Journal* **832**, p. 17 (November 2016).
52. V. S. Paliya, Fermi-Large Area Telescope Observations of the Exceptional Gamma-Ray Flare from 3C 279 in 2015 June, *Astrophysical Journal, Letters* **808**, p. L48 (August 2015).
53. M. Petropoulou, et al., A hadronic minute-scale GeV flare from quasar 3C 279?, *Monthly Notices of the RAS* **467**, L16 (May 2017).